Electron scattering in multi-wall carbon-nanotubes

Rochus Klesse
Universität zu Köln, Institut für Theoretische Physik, Zülpicher Str. 77, D-50937 Köln, Germany.
(June 14, 2002)

We analyze two scattering mechanisms that might cause intrinsic electronic resistivity in multi-wall carbon nanotubes: scattering by dopant impurities, and scattering by inter-tube electron-electron interaction. We find that for typically doped multi-wall tubes backward scattering at dopants is by far the dominating effect.

PACS

I. INTRODUCTION

Carbon nanotubes [1] appear in a rich variety of size and molecular structure. Moreover, they can self-arrange in well-defined secondary structures, like multi-wall tubes or bundles of closely packed single-wall tubes. This provides electronic systems ranging from strictly one dimensional metals and semi-conductors, up to quasi two-dimensional, graphite-like systems. Single-wall nanotubes with diameters of order nm behave even at room temperature as strictly one-dimensional electronic systems. Multi-wall tubes, on the other hand, have typically rather large diameters of several tenths of nanometers, and therefore exhibit less distinct one-dimensional features.

While it is established that the physics of a conducting single-wall tube can be described by a four-channel Luttinger liquid [2,3], the situation for multi-wall tubes is less clear from both theory and experiment. Many experiments find evidence for diffusive electronic transport [4,6,5], however, ballistic transport has been also reported [7].

The origin of the electron scattering mechanism that is at work in multi-wall tubes, but obviously inefficient in single-wall tubes, is not well understood. It could be attributed to the typically larger diameter of multi-wall tubes, which is accompanied by smaller sub-band energies. As a consequence, higher sub-bands become occupied by electrons or holes when the Fermi energy is shifted off half filling due to doping or an external electrical potential [6,8]. Unlike the two lowest bands, which are protected against backward scattering by a certain symmetry of the tube states [9], higher bands are not. They are therefore more sensitive to impurity scattering. It has been shown that this effect causes the unusually high resistivity of semi-conducting single-wall tubes [10].

Another possible scattering mechanism specific for multi-wall tubes or bundles is inter-tube Coulomb coupling. Since typically transport in such systems is supported only by a fraction of tubes [4–7], Coulomb-force mediated scattering between electrons of active and passive tubes can be a source of additional resistance as well.

In this work we analyze and compare these two scattering mechanisms. Our main result is that for multi-wall tubes with a typical amount of doping (as e.g. in [8]) backward scattering at dopants exceeds by far the backscattering caused by inter-tube electron-electron interaction.

In principle, inter-tube scattering can also be caused by incommensurate tube structures. When adjacent tubes have different molecular structure, electrons of one tube experience the static lattice potential of the other tube as incommensurate with the potential of the lattice of the own tube. As a consequence, scattering occurs. A thorough analysis of this effect, and a quantitative comparison with the aforementioned scattering processes, however, is beyond the scope of the present publication. Nevertheless, we would like to refer to recent works Ref. [11] and Ref. [12] that addresses related effects of incommensurabilities in multi-wall tubes.

In the analysis presented below we neglect inter-tube tunneling. We justify this by the fact that many experiments find evidence for that the current in a multi-wall tube flows predominantly through the outer tube [4–7]. There is also theoretical evidence that inter-tube tunneling might be strongly affected by incommensurabilities [13,12].

We begin by briefly reviewing the electronic structure of carbon nanotubes. The following section III provides the matrix elements for scattering by impurities and by electron-electron interaction. In section IV we evaluate and compare the results for real systems, and give a conclusion in section V.

II. ELECTRONIC STRUCTURE

A (n_1, n_2)-tube can be viewed as a 2D graphite lattice that is bended in a way that a lattice vector $c_{n_1,n_2} = n_1 a_1 + n_2 a_2$, where a_1, a_2 are primitive lattice vectors of length $a = 2.47\mathring{A}$, becomes a circumferential vector of a cylinder. Closing the tube periodically restricts the lattice momentum k to sub-bands defining lines $k \cdot c_{n_1,n_2} = 2\pi l$ in k-space, where the integer l is the band index [14]. Valence and conductance bands meet at the two so-called Dirac-points $K_{\alpha=\pm1}$. Tubes obeying $n_2 - n_1 = 0 \bmod 3$ have the two Dirac-points in the allowed k-space and are thus metallic, while all other tubes are semi-conducting.

In many experiments the Fermi-energy is significantly off half-filling, either due to the influence of external electrostatic potentials or doping [6,8]. The shift of the Fermi-energy is usually less than the sub-band energy separation in single-wall tubes. Hence, even in doped single-wall tubes only the lowest sub-band ($l = 0$) is occupied. Multi-wall tubes, however, have typically much larger radii and therefore much smaller sub-band energies than single-wall tubes. Consequently, the shift of the Fermi-energy usually leads to the occupation of higher sub-bands in multi-wall tubes [6,8].

The low energy physics of nanotubes is determined by electronic states in the vicinity of the Dirac-points K_α. Neglecting curvature effects, their structure can be conveniently taken from the corresponding electronic states of plane graphite: With $A_\alpha(r), B_\alpha(r)$ two degenerate, orthonormal Bloch eigenstates of 2D graphite at K_α, nearby states with momentum $k = K_\alpha + q$ can be expanded as [15,16]

$$\psi_{\alpha q} = \frac{e^{iq\cdot r_\parallel}}{\sqrt{2}} \left(A_\alpha + f_q B_\alpha\right) . \qquad (1)$$

We set $q = |q|(\cos\vartheta, \sin\vartheta)$ with respect to a fixed coordinate frame of choice. Then the relative phase is $f_q = \pm e^{i\alpha\vartheta}$ for valence band $(-)$ and conduction band $(+)$. In first order of q, the energy dispersion around K is conical [15], $E_{K+q} = \pm v_F|q|$, with $v_F \approx 5.4 eV\AA$ [17] (we use units in which $\hbar \equiv 1$ and $k_B \equiv 1$). The state $\psi_{\alpha q}$ can be viewed as a pseudo-spinor, where the two pseudo-spin polarizations refer to Bloch eigenstates A_α, B_α [16]. It is convenient to introduce a mixing angle $\gamma_{qq'}$ that measures the pseudo-spinor overlap of two states $\psi_{\alpha q}$ and $\psi_{\alpha q'}$ by

$$\cos\gamma_{qq'} = \left|\left\langle e^{-iq\cdot r_\parallel}\psi_{\alpha q}, e^{-iq'\cdot r_\parallel}\psi_{\alpha q'}\right\rangle\right| .$$

Geometrically, $\gamma_{qq'}$ is half the angle enclosed by q and q'. Eigenstates of opposite momentum have orthogonal pseudo-spin polarizations, i.e. $\gamma_{q,-q} = \pi/2$. This is the reason for the strong suppression of backscattering in metallic single-wall nanotubes [9].

The two-dimensional Bloch states (1) translate into 1D tube-states $\psi^{(l)}_{\alpha q}$ of sub-band l by

$$\psi^{(tube)}_{\alpha lk} \equiv \psi^{(gr)}_{\alpha q} , \quad q = (k, q_l) , \qquad (2)$$

where k is the momentum along the tube axis (relative to K_α) and $q_l = 2\pi l/|c_{n_1,n_2}|$ is the transversal momentum (relative to K_α) of sub-band l. The in-plane coordinates x, y and the radial coordinate z of the plane graphite-lattice coordinate frame thereby become longitudinal (x), circumferential (y), and local off-plane coordinate (z) in a curved tube coordinate frame. The coordinate y is $2\pi R$-periodic, where $2\pi R \equiv |c_{n_1,n_2}|$, and parallel to c_{n_1,n_2}.

The energy dispersion near E_F at K_- and K_+ of a sub-band l results from the dispersion $E_{K+q} = \pm v_F|q|$ confined to the line $q_y = q_l$. Hence, electrons in the lowest sub-band ($l = 0$) are massless Dirac fermions, while electrons in higher sub-bands ($l \neq 0$) acquire a mass $\Delta = v_F q_l$ (cf. figure 1). Further, in the massive bands Fermi-point states at $-k_{F,l}$ and $k_{F,l}$ have no longer orthogonal pseudo-spin polarizations, as it is the case for a massless band, but rather mix with a mixing angle

$$\gamma_{k_{F,l},-k_{F,l}} \equiv \gamma_l = \arctan k/q_l < \pi/2 .$$

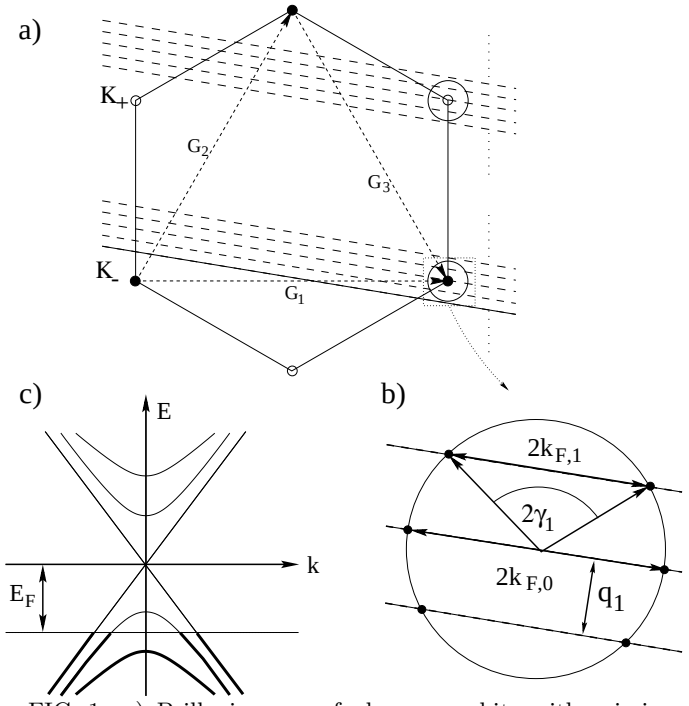

FIG. 1. a) Brillouin zone of planar graphite with primitive reciprocal lattice vectors G_1, G_2, G_3, and Dirac-points K_+ and K_-. The dashed lines (to be continued over the entire zone) represent the allowed momentum states of a metallic $(45, 15)$-carbon nanotube. Their intersections with the lines $E = E_F$ (rings around the Dirac-points) define the Fermi-points of the tube sub-bands. b) Local structure in the vicinity of K_-. c) Energy dispersion of sub-bands in the vicinity of K_-.

III. MATRIX ELEMENTS

This section provides the matrix elements for intra-sub-band backward scattering caused by interaction with dopants, and by interaction with electrons in adjacent tubes.

A. Impurity scattering

Recently, it has been observed [8] that multi-wall tubes in air are substantially hole-doped. The measured shift

of the Fermi-energy of $\Delta E \sim -0.3eV$ indicates a dopant-charge concentration of about one elementary charge per 500 carbon atoms [8]. In view of this rather high concentration, we consider dopants as the main source for inelastic scattering.

Earlier publications focused on substitutional disorder and lattice defects [20–24]. While the potentials created by these lattice imperfections vary rapidly on a scale of order or less than the lattice constant a, it is likely that the effective dopant potential $V_d(x,y)$ on the tube-surface is rather smooth on that scale. The reason for that being that the dopant might be located in a distance $b \gtrsim a$ from the tube surface and additionally may have a spatial extension. In the following we therefore assume that the dopant potential is smooth.

In this case scattering of electrons from one Dirac-point to the other is strongly suppressed [9], such that we can confine our considerations to scattering events within states in the vicinity of one Dirac-point. Following Ando et al. [9], and making use of the $k\cdot p$-approximation [15,16] we obtain for intra-sub-band backscattering the matrix element

$$\begin{aligned} M_l^{(i)} &= \int d^3r\ \psi^*_{\alpha l -k_{F,l}}(r) V_d(r) \psi_{\alpha l k_{F,l}}(r) \\ &= L^{-1} \cos\,\gamma_l\, \hat{U}_d(2k_{F,l})\,, \end{aligned} \tag{3}$$

where L is the length of the tube, and $\hat{U}_d$ the Fourier transform of the effective 1D potential

$$U_d(x) = (2\pi R)^{-1} \int_0^{2\pi R} V_d(x,y) dy\,.$$

Independent of the precise form of the dopant potential the following observations hold [9]: For a massless band ($l=0$) the matrix element vanishes, since $\cos\gamma_{l=0} = 0$ due to the orthogonality of pseudo-spin polarizations of states at $-k_{F,0}$ and $k_{F,0}$. For higher sub-bands this is not the case, and $M_l^{(i)}$ can assume appreciable values [10], depending on the mixing angle γ_l. We emphasize that typically $2k_{F,l} \ll\sim a^{-1}$, which means that the backscattering coupling $M_l^{(i)} \propto \hat{U}(2k_{F,l})$ is *not* suppressed by a large transfered momentum.

For the purpose of quantitative estimates we need to further specify the dopant potential. Modelling the dopant as an elementary charge e located in a distance b to the surface of the tube, its regularized Coulomb-potential on the tube may be written as

$$V_d(x,y) = \frac{e^2}{\sqrt{x^2 + S_{bc}(y/R)^2}}, \tag{4}$$

where $S_{bc}(\varphi)^2 = c^2 + b^2 + 4R(b+R)\sin^2(\varphi/2)$. The length c of order $1\mathring{A}$ takes into account the finite width of the graphite layer as well as the spatial extension of the dopant charge. From this potential we obtain

$$\hat{U}(q;b,c) = 2e^2 \int_0^{2\pi} \frac{d\varphi}{2\pi} K_0(q\, S_{bc}(\varphi)) \tag{5}$$

where K_0 is the modified Bessel-function of the second kind. The smoothness condition requires $(b^2+c^2)^{1/2} \gtrsim a$.

The exact values of the parameters b and c are hard to determine. Fortunately, it will turn out that the dependence on these parameters is relatively week for $(b^2+c^2)^{1/2}$ being in a rather wide regime $\approx 2.0 \cdots 10\mathring{A}$ (Sec. IV, Fig. 2). The estimates given below seem to be not very sensitive to the details of the dopant-potential, which also motivates our specific choice (4).

B. Electron-Electron scattering

The distance between adjacent walls in a multi-wall tube is as like in graphite approximately $d = 3.4\mathring{A}$. Because of this relatively large separation, we assume that the inter-tube electron-electron interaction potential can also be viewed as a smooth potential. Consequently, we will again neglect scattering transitions where electrons change from K_- to K_+, and calculate the matrix elements for the remaining backscattering events in a similar way as for the impurity scattering, as it is briefly outlined in the following.

The matrix element for inter-tube electron-electron backward scattering is

$$\begin{aligned} M_{ll'}^{(e)} = \int d^3r d^3r' \psi^*_{\alpha l k_3}(r) \psi_{\alpha l k_1}(r) V(r,r') \\ \times \psi^*_{\alpha' l' k_4}(r') \psi_{\alpha' l' k_2}(r')\,, \end{aligned}$$

where $k_1 = -k_3 \approx k_{F,l}$, $k_2 = -k_4 \approx -k_{F,l'}$, and $V(r,r')$ is the interaction potential as a function of the respective tube coordinates. Using Eq.s (2) and (1) and neglecting integrals that contain mixed terms $A^*(r)B(r)$, the matrix element becomes

$$\begin{aligned} \tfrac{1}{4} \int d^3r d^3r' (\rho_A + f_3^* f_1 \rho_B) V \times \\ (\rho'_A + f_4^* f_2 \rho'_B) \mathrm{e}^{i(k_1-k_3)x + i(k_2-k_4)x'}\,. \end{aligned}$$

Here, $\rho_{A/B}$, $\rho'_{A/B}$ denote the densities of eigenstates A and B on the two tubes. Since the transfered momentum $k_1 - k_3 = k_2 - k_4$ is small compared to a^{-1}, the microscopic structure of the densities ρ_A, ρ_B is unimportant. This allows us to approximate $\rho_{A/B}$ by a homogeneous density on the tube surface, $\rho_A = \rho_B = \delta(z)/(2\pi RL)$, and so for $\rho'_{A/B}$. In this approximation, the matrix element for backward scattering in a tube of length L is

$$M_{ll'}^{(e)} = L^{-1} \delta_{k_1-k_3, k_2-k_4} \cos\gamma_l \cos\gamma_{l'}\, \hat{U}_e(k_1-k_3)\,, \tag{6}$$

where $\hat{U}_e$ is the Fourier transform of the effective 1D electron-electron interaction potential

$$U_e(x-x') = \int_0^{2\pi R} \frac{dy}{2\pi R} \int_0^{2\pi R'} \frac{dy'}{2\pi R'} V(x-x',y,y') \, .$$

The factor $\cos\gamma_l \cos\gamma_{l'}$ in the matrix element (6) indicates the same characteristic suppression by orthogonal pseudo-spin polarizations as we have seen for the backscattering by dopants, Eq. (3). Thus, also the backscattering by electron-electron interaction vanishes for metallic bands, independently on the particular form of the interaction $V(r,r')$.

We describe the interaction between electrons on coaxial tubes of radii R and R' by the regularized Coulomb potential

$$V(x-x',y,y') = \frac{e^2}{\sqrt{(x-x')^2 + S^2_{RR'\tilde{c}}(\frac{y}{R} - \frac{y'}{R'})}} \, ,$$

where

$$S^2_{RR'\tilde{c}}(\varphi) = \tilde{c}^2 + (R-R')^2 + 4RR' \sin^2(\varphi/2) \, .$$

The parameter $\tilde{c} \sim 1\mathring{A}$ reflects the extension of the electron densities in the radial direction. For this interaction we obtain

$$\hat{U}_e(q;R,R',\tilde{c}) = 2e^2 \int_0^{2\pi} \frac{d\varphi}{2\pi} K_0(qS_{RR'\tilde{c}}(\varphi)) \, . \qquad (7)$$

The dependence of this Fourier coefficient on $\tilde{c}$ is similarly week as like the dependence of $\hat{U}_d(q;b,c)$ on c.

IV. COMPARISON

To be specific, we take parameters that are typical for the recent experiment on multi-wall nanotubes by Schönenberger et al. [6]: $D = 10nm$ for the diameter of the outer tube, and a Fermi energy $E_F = -0.3\, eV$ (relative to the energy of the Dirac-point states). Assuming a conical dispersion $E_{K_\pm+q} = v_F|q|$ with $v_F = 5.4eV\mathring{A}$, it follows that a total of $\mathcal{N} = 10$ spin-degenerate sub-bands are occupied. We label the five sub-bands at each Dirac-point by $l = 0, \pm1, \pm2$. The corresponding mixing angles are given by $\cos\gamma_l = .36\,|l|$, the $1D$-Fermi momenta are $k_{F,0} = .056\,\mathring{A}^{-1}$, $k_{F,\pm1} = .052\,\mathring{A}^{-1}$ and $k_{F,\pm2} = .039\mathring{A}^{-1}$.

The total density n_i of the dopant charges close to the tube surface can be deduced from charge neutrality [8]: the total density of electrons n_e that is expelled from the tube in its neutral state (where $E_F = 0$) must equal the density n_i of dopants. For the chosen parameters we find $n_e = n_i = 3.0nm^{-1}$.

The efficiency of the two scattering mechanisms under discussion cannot be directly compared by their matrix elements presented in the previous section. A quantity that is suited for a comparison is for example the transport scattering time τ. To proceed with a reasonable amount of effort, we calculate τ within the scope of a Boltzmann-equation approach [19], where we restrict ourself to inter-sub-band scattering only.

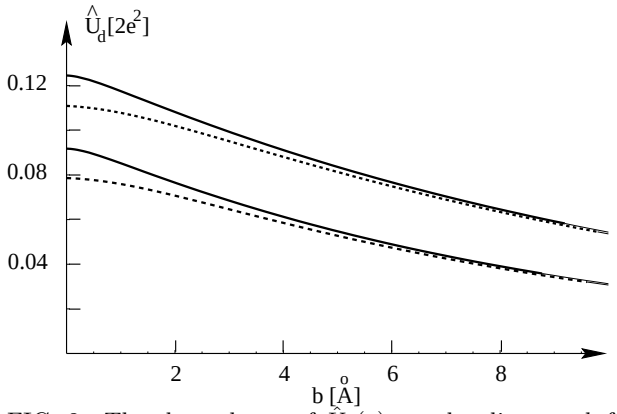

FIG. 2. The dependence of $\hat{U}_d(q)$ on the distance b for parameter $c = 0.5\mathring{A}$ (dashed) and $c = 2.0\mathring{A}$ (solid). The wavevectors are choosen to be $q = 2k_{F,1}$ for the lower, and $q = 2k_{F,2}$ for the upper curves.

For scattering at dopants we find in this way

$$\frac{1}{\tau_l^{(i)}} = \frac{2n_i}{v_{F,l}} |LM_l^{(i)}|^2 \qquad (8)$$

$$= \frac{2n_i}{v_{F,l}} \cos^2\gamma_l \, |\hat{U}(2k_{F,l};b,c)|^2 \, . \qquad (9)$$

The dependence of $\hat{U}(q;b,c)$ (Eq.(5)) on the parameters b and c is rather weak, as shown in Fig. 2. For transfered momenta $q = 2k_{F,1/2}$ the potential $\hat{U}$ varies with b and c ranging from $2.0 \cdots 10\mathring{A}$ and $0.5 \cdots 2\mathring{A}$ by less than a factor of 3. The transport scattering times in this range of parameters are

$$\frac{1}{\tau_0^{(i)}} = 0, \quad \frac{1}{\tau_1^{(i)}} = .012 \cdots 0.076\, eV, \quad \frac{1}{\tau_2^{(i)}} = .20 \cdots 0.82\, eV \, , \qquad (10)$$

where the lower values belongs to $b = 10\mathring{A}$ and $c = 2.0\mathring{A}$, the higher to $b = 2.0\mathring{A}$ and $c = 0.5\mathring{A}$. The corresponding mean free paths, formally defined by $l_l \equiv v_{F,l}\tau^{(i)}$, are $l_0 = \infty$, $l_1 = 0.66 \cdots 41nm$, and $l_2 = .46 \cdots 1.9nm$.

The rather large values of the inverse transport times for $l = 1$ and 2 indicate that as soon as massive bands are involved, backscattering at dopants indeed gives rise to a significant intrinsic resistivity. Taking the calculated mean free paths l_1 and l_2 literally would even result in a higher resistivity than is actually observed [5,6]. The reason for this overestimation could be an improper modelling of the dopant impurities or the neglect of screening.

For the transport time caused by backscattering of electrons in sub-bands l and l' of different tubes we obtain within the Boltzmann-equation approach

$$\frac{1}{\tau^{(e)}_{ll'}} = \frac{T}{2\pi v_{F,l} v_{F,l'}} |L M^{(e)}_{ll'}|^2 \qquad (11)$$
$$= \frac{T}{2\pi v_{F,l} v_{F,l'}} \cos^2\gamma_l \cos^2\gamma_{l'} |\hat{U}_e(2k_{F,l}; R, R', \tilde{c})|^2 \, .$$

Here it is assumed that the Fermi-momenta in the participating channels match, $k_{F,l} = k_{F,l'}$, otherwise the scattering rate is strongly suppressed (see Eq. (6)).

Evaluating Eq. (11) for $R = 50\mathring{A}$, $R' = R - 3.4\mathring{A}$, and $\tilde{c} = 1.0\mathring{A}$, we obtain in this case the transport scattering times

$$\frac{1}{\tau^{(e)}_{00}} = 0, \quad \frac{1}{\tau^{(e)}_{11}} = 4.3\,10^{-4} T \, , \quad \frac{1}{\tau^{(e)}_{22}} = .028\, T \, . \qquad (12)$$

Even at room temperature these inverse transport times are by orders of magnitude smaller than those caused by dopant scattering. This strong suppression is mainly due to the smallness of the dimensionless parameter $T \,/\, v_F n_i \sim \pi T \,/\, \mathcal{N}|E_F|$. (The matrix elements $M^{(e)}_{ll}$ and $M^{(i)}_{l}$ are of comparable size.) Interpreting the inverse thermal wavelength as the density n_T of thermally activated electrons/holes, $n_T = T/v_F$, the small value of $\tau^{(i)}/\tau^{(e)}$ corresponds to the fact that for the considered parameters the density n_i exceeds n_T by a large factor $\mathcal{N}|E_F| \,/\, \pi T$.

V. DISCUSSION

The preceding estimates show that under typical experimental conditions scattering by dopants can be a source of significant intrinsic resistance in multi-wall nanotubes.

The typically larger diameter of multi-wall tubes entails the occupation of higher sub-bands, which are, in contrast to the massless sub-bands ($l = 0$), no longer protected against backscattering by orthogonal pseudospin polarizations of states at opposite Fermi-points. The same effect explains [10] the high resistivity of gated semiconducting single-wall nanotubes, which naively could be expected to be as well conducting as metallic single-wall tubes. In fact, it has been already speculated in Ref. [10] that the resistance of multi-wall tubes could have the same origin.

The conclusion that the enhancement of backscattering in multi-wall tubes is due to their larger radii is not at odds with the results of White and Todorov [22]. Their observation that impurity scattering decreases with increasing diameter of tube applies for scattering within the *massless* bands, while our conclusion relies on the investigation of backscattering in the *massive* bands.

For Coulomb interaction with electrons in inner tubes we observe a qualitatively similar behaviour: the suppression of backscattering in the massless bands due to anti-symmetry is suspended in the massive bands. Quantitatively, we find however that for a typicall amount of doping [8] the backscattering rate caused by intra-tube electron-electron interaction is by orders of magnitudes smaller than the rate caused by the interaction with dopants.

Combining these two results, on might say that the observed non-ballistic electronic transport in multi-wall tubes is primarily due to the enhanced backscattering at dopant impurities, and not an effect of interactions between different shells.

The reported ballistic transport in multi-wall tubes in the experiment by Frank et al. [7] does not contradict the picture presented here. Differing from the others, in this experiment the tubes have been contacted by partially immersing them into liquid mercury. Thereby the tubes may have been cleaned from surface impurities and may have been also protected from absorbing surface dopants [7]. For this reason, in this experiment the Fermi-energy may be close to the energy of the Dirac points, such that only the massless bands are occupied (for which backscattering by impurities or electrons in other shells is suppressed). Or, even when higher bands are occupied, due to the absence of surface impurities backscattering is insignificant.

The intra-sub-band scattering rate has been considered as an indicator for the strength of two certain scattering mechanisms. For a more quantitative comparison with experimental results it is necessary to include also (back)scattering between different sub-bands. Further improvements might be achieved by a more precise modelling of the dopant potential, and taking into account effects of screening and electronic correlations.

Finally, we like to stress that the present work focused on impurity- and electron-electron scattering only. For a complete picture of the transport in nanotubes it is necessary to investigate other possible scattering mechanisms. Particularly, further investigations of the effects of lattice incommensurabilities on transport are desirable.

I thank S. Ernst for critically reading the manuscript.

[1] S. Iijima, Nature **354**, 56 (1991).
[2] R. Egger and A. O. Gogolin, Phys. Rev. Lett. **79**, 5082 (1997); C. L. Kance, L. Balents, and M. P. A. Fisher, Phys. Rev. Lett. **79**, 5086 (1997); Z. Yao, H. Postma, L. Balents, and C. Dekker, Nature **402**, 273 (1999); H. Postma, T. Teepen, Z. Yao, M. Grifoni, and C. Dekker, Science **293**, 76 (2001).
[3] M. Bockrath, D. H. Cobden, J. Lu, A. G. Rinzler, R. E. Smalley, L. Balents, Paul L. McEuen, Nature (London) **397**, 598 (1999).
[4] L. Langer, V. Bayot, E. Grivei, J.-P. Issi, J. P. Here-

mans, C. H. Olk, L. Stockman, C. Van Haesendonck, Y. Bruynseraede, Phys. Rev. Lett. **76**, 479 (1996).
[5] A. Bachtold, C. Strunk, J.-P. Salvetat, J.-M. Bonard, L. Forr, T. Nussbaumer, C. Schnenberger, Nature **397**, 673 (1999).
[6] C. Schönenberger, A. Bachtold, C. Strunk, J.P. Saletat, L. Forroó, Appl. Phys. A **69**, 283 (1999).
[7] S. Frank, P. Poncharal, Z. L. Wang, and W. A. de Heer, Science **280**,1744 (1998).
[8] C. Schönenberger, M. Buitelaar, M. Krüger, I. Widmer, T. Nussbaumer, and M. Iqbal, Proceedings Moriond 2001 (cond-mat/0106501); M. Krüger, M. Buitelaar, T. Nussbaumer, C. Schönenberger, Appl. Phys. Lett. **78**, 1291 (2001).
[9] T. Ando, T. Nakanishi, and R. Saito, J. Phys. Soc. Japan, **67**, 2857 (1998); T. Ando and T. Nakanishi, J. Phys. Soc. Japan, **67**, 1704 (1998).
[10] P. L. McEuen, M. Bockrath, D. H. Cobden, Y.-G. Yoon, S. G. Louie, Phys. Rev. Lett. **83**, 5098 (1999).
[11] A. N. Kolmogorov and V. H. Crespi, Phys. Rev. Lett. **85**, 4727 (2000) investigate the effect of incommensurate tube-structures on interlayer sliding in multi-wall tubes.
[12] S. Roche, F. Triozon, A. Rubio, D. Mayou, Physics Letters A, **285**, 94 (2001), S. Roche, F. Triozon, A. Rubio, and D. Mayou, Phys. Rev. B **64**, 121401 (2001) study the effect of inter-tube tunneling and diffusion on transport in incommensurate, disorder-free multi-wall tubes.
[13] A. A. Maarouf, C. L. Kane, and E. J. Mele, Phys. Rev. B **61**, 11156 (2000).
[14] R. Saito, M. Fujita, G. Dresselhaus, and M. S. Dresselhaus, Appl. Phys. Lett. **60**, 2204 (1992).
[15] J. C. Slonczewski and P. R. Weiss, Phys. Rev. **109**, 272 (1958).
[16] D. P. DiVincenzo and E. J. Mele, Phys. Rev. B **29**, 1685 (1984).
[17] G. S. Painter and D. E. Ellis, Phys. Rev. B **1**, 4747 (1970).
[18] P. R. Wallace, Phys. Rev. **71**, 622 (1947).
[19] see e.g. A. A. Abrikosov, *The Theory of Normal Metals*, Hindustan Publishing Corporation (India) 1968.
[20] L. Chico, L. X. Benedict, S. C. Louie, A. L. Cohen, Phys. Rev. B **54**, 2600 (1996); Phys. Rev. B **61**, 10511 (2000).
[21] Ryo Tamura and Masaru Tsukada, Phys. Rev. B **55**, 4991 (1997).
[22] C. T. White and T. N. Todorov, Nature **393**, 240 (1998).
[23] M. P. Anatram and T. R. Govindan, Phys. Rev. B **58**, 4882 (1998).
[24] T. Kostyrko, M. Bartkowiak, G. D. Mahan, Phys. Rev. B **60**, 10735 (1999).
[25] A. Bachtold et al., Phys. Rev. Lett. **84**, 6082 (2000).